JOURNAL OF COMPUTATIONAL PHYSICS 104, 75–85 (1993)

# A Computational Study of the Dynamical Evolution of Self-Gravitating Systems

G. YEPES

*Canadian Institute for Theoretical Astrophysics, University of Toronto, 60 St. George Street, Toronto, Ontario, Canada M5S 1A7*

AND

R. DOMÍNGUEZ-TENREIRO

*Departamento de Física Teórica C-XI, Universidad Autónoma de Madrid, Cantoblanco-28049, Madrid, Spain*

Received July 23, 1991; revised March 2, 1992

We have developed a computing procedure to study the dynamical evolution of self-gravitating astronomical systems. It is based on a stochastic model which is a generalization to the multimass and anisotropic case of the Fokker–Planck equation moment method. In this paper we present the main characteristics of the model and the computing procedure. We also present a practical application of the method.


## 1. INTRODUCTION

The dynamical evolution of self-gravitating $N$ body systems, with large $N$, such as star clusters, galactic nuclei, galaxies and, rich galaxy clusters, is a long standing problem in astronomy, which has only been partially solved with the help of some fairly strong simplified assumptions. The problem is, nevertheless, outstanding because there are at present some open questions, such as the time scales for the evolution of these systems and their dependence on their particular characteristics, whose solution is fundamental in order to correctly interpret some observations (luminosity segregation in galaxy clusters, the origin of the huge energy emission from active galactic nuclei, etc.). There is now a general agreement that two different stages can be distinguished in the dynamical evolution of self-gravitating systems: first, a fast phase, where the dynamics is controlled by a collective potential (violent relaxation); then a slow phase, where binary collisions play the prevailing role (two-body relaxation).

From a theoretical point of view, there exist two main categories of methods to follow the time evolution of self-gravitating systems: (1) $N$-body simulations [1–3] which describe both phases of evolution; (2) statistical methods based on the Fokker–Planck equation formalism to describe the evolution of the distribution function. These methods cover the two-body relaxation phase. The Fokker–Planck equation can be numerically solved through different methods, such as Monte Carlo simulations [4–7], direct integration of the equation in the orbit-averaged approximation [8–12], and the moment method [14–21].

At present most authors agree that there exists a nonluminous gravitating matter which could possibly dominate the dynamical behavior of astronomical objects at large scale, as implied by the increase of the mass-luminosity relation of these objects with the scale detected in astronomical observations. The problem of the microphysical nature of these dark matter particles is an open question. In standard cosmologies, an important fraction of the dark matter must be non-baryonic [22, 23]. In any case and irrespective of their microphysical properties, dark matter particles are likely to be much lighter than a typical star or galaxy, their number density much higher than the typical densities of stars in a cluster or in galaxies, or of galaxies in a cluster, and to interact mainly gravitationally.

The present-day generation of computers is unable to properly simulate the dynamical evolution of a self-gravitating systems endowed with a background of light and abundant particles by means of $N$-body techniques. We have to resort to statistical methods. Unfortunately, the Fokker–Planck equation is difficult to solve, so that works found in literature on this subject have only taken into account some simplified versions of the problem, such as a monomass spherical configuration with isotropic distribution function [6, 9] (in the momentum space), anisotropic distribution, and a monomass system [12, 15], or isotropic distributions with a mass spectrum, either in the local [17] or in the orbit-averaged approximations [11, 13].



0021-9991/93 $5.00

In contrast with this situation, any simulation of the dynamical evolution of self-gravitating systems which tries to be somehow realistic, has to simultaneously include anisotropic distribution functions and a mass spectrum. The approximation of isotropy fails because two-body relaxation effects give rise to an anisotropy development, as has been shown for a monomass system [12]. Concerning the mass spectrum, astronomical self-gravitating objects are not monomass systems because, apart from the background of light particles, they are made of stars or galaxies of different masses. This is particularly important in galaxy clusters, where the mass of individual galaxies can vary by three orders of magnitude or more.

We have developed a statistical model to study the evolution of self-gravitating systems which takes into consideration, at the same time, the existence of a mass spectrum and allows for anisotropy in the distribution functions. The Fokker–Planck equation has been solved by means of the moment method, which has been chosen because of its computational economy. This allows us to perform a detailed analysis of the influence of the initial conditions on the dynamical evolution of the system. At this moment, we have applied our model to the study of the evolution of rich galaxy clusters. The results of this study, presented elsewhere [20, 21], suggest that some observational features of these systems, such as the luminosity segregation and the central decrease in the projected profile of the velocity dispersion for the most massive galaxies, can be interpreted as due to the dynamical evolution in the two-body relaxation phase and that the observed differences among different clusters are a result of the different conditions at the onset of this evolutionary phase, as described by different values of the parameters of the model.

In this paper we present the numerical procedure employed to solve the model and the main characteristics of the code we have developed to this end. Also, in order to underline the relevance of our assumptions, some results of the computations are presented.

The paper is organized as follows: in Section 2 the multimass anisotropic model for the evolution of self-gravitating systems is described. Section 3 deals with the numerical method to solve the model. In Section 4 we show some results of the computations. Finally, Section 5 is devoted to the summary and conclusions.

## 2. DESCRIPTION OF THE MODEL

Let us consider a system of self-gravitating particles composed of $N$ different subsystems of equal mass particles, $m_a$. In each subsystem we define a distribution function, $f^a(\mathbf{r}, \mathbf{v}, t)$. The dynamical evolution of these distribution functions, due to binary collisions, is described by the Boltzmann equation with collision term:

$$\frac{\partial f^a}{\partial t} + \mathbf{v} \cdot \nabla_{\mathbf{r}} f^a + \nabla_{\mathbf{r}} \Phi \cdot \nabla_{\mathbf{v}} f^a = \left.\frac{df^a}{dt}\right|_{\text{coll}}, \tag{1}$$

where $\Phi$ is the total gravitational potential and $df^a/dt|_{\text{coll}}$ gives the change of $f^a(\mathbf{r}, \mathbf{v}, t)$ due to binary encounters with all the other particles in the system.

In order to simplify the problem, we assume that the system is spatially spherical symmetric and axially symmetric around the radial direction in the momentum space. If we define the average value of the function $A$ in the subsystem "$a$" by

$$\langle A \rangle_a = \frac{\int d^3\mathbf{v}\, A f^a(\mathbf{r}, \mathbf{v}, t)}{\int d^3\mathbf{v}\, f^a(\mathbf{r}, \mathbf{v}, t)} \tag{2}$$

then the distribution functions are characterized by the moments [14]

$$\rho_a \equiv \langle M \rangle_a \tag{3}$$

$$\bar{u}_a \equiv \langle u \rangle_a \tag{4}$$

$$\alpha_a \equiv \langle (u - \bar{u}_a)^2 \rangle_a \tag{5}$$

$$\beta_a \equiv \langle v^2 \rangle_a = \langle w^2 \rangle_a \tag{6}$$

$$\varepsilon_a \equiv \langle (u - \bar{u}_a)^3 \rangle_a \tag{7}$$

$$\zeta_a \equiv \langle (u - \bar{u}_a)^4 \rangle_a \tag{8}$$

$$\xi_a \equiv \zeta_a - 3\alpha_a^2 \tag{9}$$

with $u$ being the radial velocity and $v$ and $w$ the transverse velocities. Due to the symmetries of the system, the odd moments of the transverse velocities are zero:

$$\langle v^{2n+1} \rangle = \langle w^{2n+1} \rangle = 0. \tag{10}$$

In Eqs. (3)–(9) $\rho_a$ is the mass density of particles $a$, $\bar{u}_a$ their mean radial velocity, $\alpha_a$ and $\beta_a$ are their velocity dispersion in the radial and transverse directions (they are identical in the isotropic case), $\varepsilon_a$ is the skewness of the distribution and it measures the energy flux, $\zeta_a$ is the kurtosis of the distribution, and $\xi_a$ is the excess coefficient, which gives a measure of the peakness of the distribution relative to a gaussian: when $\xi_a > 0$ there exists an excess of low velocity type $a$ particles with respect to a gaussian distribution, and conversely if $\xi_a < 0$.

The moment method to solve the Boltzmann equation (1) consists of taking its moments and to solve the resulting set of moment equations instead of the Eq. (1). When this is done, in the equation for the $n$th moment appears the $(n+1)$th moment, so that we are left with an infinite number of moment equations. In practice, however, an approximation is made and only a finite number are taken into consideration by cutting the hierarchy. It is known that

the third-order moment, $\varepsilon_a$, plays an essential role in the evolution of self-gravitating systems [14, 15, 24] and we need to know the evolution of $\zeta_a$ in order to have a significant insight into the $\varepsilon_a$ evolution, so that we have to consider, at least, up to the fourth-order moment, $\zeta_a$. Moreover, due to the anisotropy in the momentum space of the distribution function, in the evolution equations for the first four moments, some mixed moments of radial and tangential components appear as well as moments of fifth order, so that, in order to close the system, an additional hypothesis concerning the physical nature of the dynamical evolution has to be made. In accordance with Larson [14], which studied the monomass case, we have assumed that the distribution functions for any subsystem remain close to a (isotropic) Maxwellian along the evolution, so that we can expand the difference in Legendre polynomials and write (we assume the $f^a$ has been normalized to unity):

$$f^a(V,\mu) = g^a(V) + \sum_{n=0}^{l} a_n^a(V)\, P_n(\mu), \tag{11}$$

where $V$ is the magnitude of the random velocity vector relative to $\bar{u}_a$, $\mu$ is the cosine of the angle between this vector and the radial direction, $P_n(\mu)$ is the Legendre polynomial of order $n$, and

$$g^a(V) = (2\pi b_a)^{-3/2} \exp(-V^2/2b_a). \tag{12}$$

where $b_a$ is a measure of the average kinetic energy of type $a$ particles in the Maxwellian distribution and has been taken to be equal to the second moment of the $f^a$ distribution:

$$b_a = \frac{\alpha_a + 2\beta_a}{3}. \tag{13}$$

Because the second term in the r.h.s. of Eq. (11) has been assumed to be always small, the expansions into Legendre polynomials can be cut at a finite order $l$. If one wants to properly represent all the dynamical characteristics of a self-gravitating system, the expansion has to be led up to order $l = 2$ at least. Also, the coefficients $a_n^a$ can be considered to be small corrections to $g^a(V)$ and expanded as a power series in $V$.

The simplest expressions for these coefficients leading to nonzero values for the anisotropy $\alpha_a - \beta_a$, the heat flux $\varepsilon_a$, and the $\xi_a$ moment, and which satisfy Eq. (13) and the conditions

$$\int dV\, d\mu\, f^a(V,\mu) = 1 \tag{14}$$

$$\int dV\, d\mu\, V\, \mu f^a(V,\mu) = 0 = \langle u - \bar{u}_a \rangle_a \tag{15}$$

are

$$a_0^a(V) = g^a(V)\, c_0^a \left[1 - \frac{2}{3b_a} V^2 + \frac{1}{15 b_a^2} V^4\right] \tag{16}$$

$$a_1^a(V) = g^a(V)\, c_1^a \frac{V}{b_a^{1/2}} \left[-1 + \frac{1}{5b_a} V^2\right] \tag{17}$$

$$a_2^a(V) = g^a(V)\, c_2^a \frac{V^2}{b_a}. \tag{18}$$

The $c_n^a$ coefficients can be calculated by introducing expressions (16)–(18) into Eq. (11) and then into Eqs. (3)–(9). The result is

$$c_0^a = \frac{5}{8} \frac{\xi_a + 4(\alpha_a - \beta_a)^2/3}{b_a^2} \tag{19}$$

$$c_1^a = \frac{5\varepsilon_a}{6 b_a^{3/2}} \tag{20}$$

$$c_2^a = \frac{\alpha_a - \beta_a}{3b_a}. \tag{21}$$

In previous works on the anisotropic moment method, the population of target particles has been considered to be isotropic in the momentum space [14, 16]. This considerably simplifies the calculations. But for the multimass case this approximation results in the inconsistency that the total momentum is not conserved, so that it is not correct. In this work, the expansion in Legendre polynomials has been led up to order $l = 2$ for both test and target particles. In this way the total momentum is conserved (see below) and the anisotropy is treated in a self-consistent manner.

We would like to point out that, according to Eqs. (16)–(18), the closure hypothesis is verified as long as the dimensionless functions $c_n^a \ll 1$ for $n = 0, 1, 2$ at any time. Within this approximation, the evolution equations for the moments of the distribution function can be put in terms of the first four moments given in Eqs. (3)–(9) and the system is closed. The resulting set of moment equations for each subsystem is

$$\frac{\partial \rho_a}{\partial t} + \frac{1}{r^2} \frac{\partial}{\partial r} [r^2 \rho_a \bar{u}_a] = 0 \tag{22}$$

$$\frac{\partial \bar{u}_a}{\partial t} + \bar{u}_a \frac{\partial \bar{u}_a}{\partial r} + \frac{1}{\rho_a} \frac{\partial}{\partial r} [\rho_a \alpha_a] + \frac{2(\alpha_a - \beta_a)}{r} + \frac{d\Phi}{dr} = \left.\frac{d\bar{u}_a}{dt}\right|_{\text{coll}} \tag{23}$$

$$\frac{\partial \alpha_a}{\partial t} + \bar{u}_a \frac{\partial \alpha_a}{\partial r} + 2\alpha_a \frac{\partial \bar{u}_a}{\partial r} + \frac{1}{\rho_a} \frac{\partial}{\partial r} [\rho_a \varepsilon_a] + \frac{2\varepsilon_a}{r}\left(1 - \frac{2\beta_a}{3\alpha_a}\right) = \left.\frac{d\alpha_a}{dt}\right|_{\text{coll}} \tag{24}$$

$$\frac{\partial \beta_a}{\partial t}+\bar{u}_a\frac{\partial \beta_a}{\partial r}+\frac{1}{3\rho_a}\frac{\partial}{\partial r}\left[\frac{\beta_a}{\alpha_a}\rho_a\varepsilon_a\right]+\frac{2\beta_a\bar{u}_a}{r}+\frac{4\beta_a\varepsilon_a}{3\alpha_a r}=\left.\frac{d\beta_a}{dt}\right|_{\text{coll}} \tag{25}$$

$$\frac{\partial \varepsilon_a}{\partial t}+\bar{u}_a\frac{\partial \varepsilon_a}{\partial r}+3\varepsilon_a\frac{\partial \bar{u}_a}{\partial r}+3\alpha_a\frac{\partial \alpha_a}{\partial r}+\frac{1}{\rho_a}\frac{\partial}{\partial r}[\rho_a\xi_a]+\frac{2\xi_a}{r}\left(1-\frac{\beta_a}{\alpha_a}\right)=\left.\frac{d\varepsilon_a}{dt}\right|_{\text{coll}}-3\alpha_a\left.\frac{d\bar{u}_a}{dt}\right|_{\text{coll}} \tag{26}$$

$$\frac{\partial \xi_a}{\partial t}+\bar{u}_a\frac{\partial \xi_a}{\partial r}+4\xi_a\frac{\partial \bar{u}_a}{\partial r}+6\varepsilon_a\frac{\partial \alpha_a}{\partial r}+4\alpha_a\frac{\partial \varepsilon_a}{\partial r}=\left.\frac{d\xi_a}{dt}\right|_{\text{coll}}-4\varepsilon_a\left.\frac{d\bar{u}_a}{dt}\right|_{\text{coll}}. \tag{27}$$

To these equations we have to add the Poisson equation for the gravitational potential, $\Phi(r)$,

$$\frac{1}{r^2}\frac{d}{dr}\left[\frac{r^2\,d\Phi}{dr}\right]=4\pi G\sum_{b=1}^{N}\rho_b. \tag{28}$$

Let us now consider the effects of binary encounters between particles on the distribution functions, described by the r.h.s. of Eq. (1). In a system with a large number of particles, these effects constitute a markovian stochastic process [25] and can be mathematically described by the Fokker–Planck equation, which in the local approximation is [26]

$$\left.\frac{df^a(\mathbf{v})}{dt}\right|_{\text{coll}}=-\sum_{i=1}^{3}\frac{\partial}{\partial v_i}(f^a\langle\Delta v_i\rangle_a)+\frac{1}{2}\sum_{i,j=1}^{3}\frac{\partial^2}{\partial v_i\partial v_j}(f^a\langle\Delta v_i\,\Delta v_j\rangle_a), \tag{29}$$

where the diffusion coefficients are given by

$$\langle\Delta v_i\rangle_a=\sum_{b=1}^{N}\Gamma_{ab}\frac{\partial}{\partial v_i}\mathscr{H}_{ab}, \tag{30}$$

$$\langle\Delta v_i\,\Delta v_j\rangle_a=\sum_{b=1}^{N}\Gamma_{ab}\frac{\partial^2}{\partial v_i\,\partial v_j}\mathscr{G}_b. \tag{31}$$

They represent the average change in the velocity of type $a$ particles due to collisions with target particles of any type. In Eqs. (30) and (31) $\Gamma_{ab}$ is given by

$$\Gamma_{ab}\equiv 4\pi G^2 m_b^2\ln\left[\frac{D_{\max}\langle V^2\rangle_a}{G(m_a+m_b)}\right] \tag{32}$$

with $G$ the Newton constant and $D_{\max}$ the maximum impact parameter, taken to be the largest dimension of the system. The functions $\mathscr{H}_{ab}$ and $\mathscr{G}_b$ are the Rosenbluth potentials [27]. They are defined as

$$\mathscr{H}_{ab}\equiv\frac{m_a+m_b}{m_b}\int d^3\mathbf{v}'\frac{f^b(\mathbf{v})}{|\mathbf{v}-\mathbf{v}'|} \tag{33}$$

$$\mathscr{G}_b\equiv\int d^3\mathbf{v}'\,f^b(\mathbf{v})\,|\mathbf{v}-\mathbf{v}'|. \tag{34}$$

Expanding the distribution function for target particles, $f^b$, as explained above (Eqs. (11) and (16)–(18)) up to $l=2$, we obtain the following expressions for the collision terms (for further details on the calculation see Ref. [28].)

$$\left.\frac{d\bar{u}_a}{dt}\right|_{\text{coll}}=\sum_{b=1}^{N}\left(1+\frac{m_a}{m_b}\right)\frac{\varepsilon_a-\varepsilon_b}{T_{ab}(b_a+b_b)} \tag{35}$$

$$\begin{aligned}\left.\frac{d\alpha_a}{dt}\right|_{\text{coll}}=&-2b_a\sum_{b=1}^{N}\frac{1}{T_{ab}}\left\{\frac{m_a}{m_b}+\frac{c_0^a b_a}{(b_a+b_b)^2}\times\left(\frac{m_a}{m_b}\frac{b_a-4b_b}{5}-b_b\right)\right\}\\&+2\sum_{b=1}^{N}\frac{b_b}{T_{ab}}\left\{1+\frac{c_0^b b_b}{(b_a+b_b)^2}\times\left(\frac{b_b-4b_a}{5}-\frac{m_a}{m_b}b_a\right)\right\}\\&-\frac{2}{5}c_2^a b_a\sum_{b=1}^{N}\frac{1}{T_{ab}}\times\left\{\frac{(2b_a+5b_b)(2(m_a/m_b)+3)-3b_b}{(b_a+b_b)}\right\}\\&+\frac{2}{5}\sum_{b=1}^{N}\frac{c_2^b b_b}{T_{ab}}\left\{\frac{b_a(6((m_a/m_b)+1/2)-b_b}{(b_a+b_b)}\right\}\end{aligned} \tag{36}$$

$$\begin{aligned}\left.\frac{d\beta_a}{dt}\right|_{\text{coll}}=&\left.\frac{d\alpha_a}{dt}\right|_{\text{coll}}+\frac{6}{5}c_2^a b_a\sum_{b=1}^{N}\frac{1}{T_{ab}}\\&\times\left\{\frac{(2b_a+5b_b)(2(m_a/m_b)+3)-3b_b}{(b_a+b_b)}\right\}\\&-\frac{6}{5}\sum_{b=1}^{N}\frac{c_2^b b_b}{T_{ab}}\left\{\frac{b_a(6(m_a/m_b)+1/2)-b_b}{(b_a+b_b)}\right\}\end{aligned} \tag{37}$$

$$\left.\frac{d\varepsilon_a}{dt}\right|_{\text{coll}} = \frac{6\varepsilon_a}{5}\sum_{b=1}^{N}\frac{1}{T_{ab}}$$

$$\times\left\{\frac{(b_a^2/6)-(13b_b^2/3)-(5b_ab_b/12)}{-(m_a/m_b)((5b_b^2/2)-(b_a^2/2)-(7b_ab_b/4))}{(b_a+b_b)^2}\right\}$$

$$+\frac{6}{5}\sum_{b=1}^{N}\frac{\varepsilon_b}{T_{ab}}\left\{\frac{b_a^2-(11b_ab_b/4)+(m_a/m_b)(5b_a^2/2)}{-(5b_ab_b/4))}{(b_a+b_b)^2}\right\} \tag{38}$$

$$\left.\frac{d\xi_a}{dt}\right|_{\text{coll}} = -\frac{12}{5}\sum_{b=1}^{N}\frac{b_a(2b_a+5b_b)}{T_{ab}}\left\{\frac{(m_a/m_b)\,b_a-b_b}{(b_a+b_b)}\right\}$$

$$+\frac{4}{25}c_0^a b_a^2\sum_{b=1}^{N}\frac{1}{T_{ab}}\left\{\frac{1}{(b_a+b_b)^3}\right.$$

$$\left.\times\left[\begin{matrix}(m_a/m_b)(2b_a^3+9b_a^2b_b+72b_ab_b^2-40b_b^3)\\+3b_b(2b_a^2+9b_ab_b-28b_b^2)\end{matrix}\right]\right\}$$

$$-\frac{12}{5}\sum_{b=1}^{N}\frac{c_0^b b_b^2}{T_{ab}}$$

$$\times\left\{\frac{b_a((m_a/m_b)\,b_a(5b_b-2b_a)-b_b(b_b-6b_a))}{(b_a+b_b)^3}\right\}$$

$$-\frac{24}{35}c_2^a b_a\sum_{b=1}^{N}\frac{b_a+b_b}{T_{ab}}\left\{\frac{1}{(b_a+b_b)^3}\right.$$

$$\left.\times\left[\begin{matrix}2(m_a/m_b)\,b_a(8b_a^2+28b_ab_b+35b_b^2)\\+(12b_a^3+31b_a^2b_b+14b_ab_b^2-35b_b^3)\end{matrix}\right]\right\}$$

$$+\frac{24}{35}\sum_{b=1}^{N}\frac{c_2^b b_b(b_a+b_b)}{T_{ab}}$$

$$\times\left\{\frac{3(m_a/m_b)b_a^2(7b_b-3b_a)+25b_a^2b_b-7b_ab_b^2+2b_a^3}{(b_a+b_b)^3}\right\}$$

$$-6\alpha_a\left.\frac{d\alpha_a}{dt}\right|_{\text{coll}} \tag{39}$$

In these expressions $T_{ab}$ is defined as

$$T_{ab}\equiv\frac{3}{4(2\pi)^{1/2}}\frac{(b_a+b_b)^{3/2}}{G^2m_b\rho_b\ln[(3D_{\max}b_a/G(m_a+m_b))]}; \tag{40}$$

it has the dimension of time and can be taken as a measure of the relaxation time of test $a$ particles colliding with a background of target $b$ particles.

## 3. NUMERICAL METHOD AND COMPUTING CODE CHARACTERISTICS

The set of Eqs. (22)–(27) with collision terms given by Eqs. (35)–(39), characterizing the evolution of the moments of the distribution function for type $a$ particles, with $a = 1, 2, ..., N$, form a system of $6 \times N$ nonlinear equations in partial derivatives (in $r$ and $t$) which, in addition to the Poisson equation (28), describe the dynamical evolution of the self-gravitating system. The equations for the different particle types are coupled through the collision terms and the Poisson equation.

We have developed a numerical code to solve the full set of equations for an arbitrary number of mass subsystems. The procedure we have used is similar to the numerical methods employed in hydrodynamical problems with spherical symmetry. As in these cases, an Eulerian scheme in difference equations proves to be the most appropriate to obtain a numerical solution of the system (22)–(27).

The difference equations have been written in an implicit form, backwards in time, in order to ensure the numerical stability and to avoid the Courant condition [29]. This allows us to use time steps considerably larger than in the case of explicit methods.

In order to make the computations easier, it is advantageous to replace Eqs. (22) and (28), introducing the auxiliary variable $M_a(r)$:

$$\frac{\partial M_a}{\partial r} = 4\pi r^2\rho_a \tag{41}$$

$$\frac{\partial M_a}{\partial t} = -4\pi r^2\rho_a\bar{u}_a. \tag{42}$$

The grid points in $r$ have been taken to be spaced at equal logarithmic intervals $\Delta \log r$. In writing the difference equations, odd moments $\bar{u}_a$, $\varepsilon_a$ and the auxiliary mass $M_a(r)$ have been evaluated at the grid points $r_i$, while the even moments $\rho_a$, $\alpha_a$, $\beta_a$, and $\xi_a$ at points in between: $r_{i-1/2} \equiv 1/2(r_i + r_{i-1})$. In this way, the spatial gradients of the different moments are centered with respect to the grid points, where the moments are evaluated.

There is a considerable arbitrariness to translate the equations in partial derivatives into difference equations, and only by putting different schemes to the test can one find out which is the most suited to a particular problem. The set of difference equations we have chosen is based on previous studies [14] for the monomass case. They are

$$M_i^a = (M_i^a)^n - 4\pi r_i^2(\rho_{i-1/2}^a\rho_{i+1/2}^a)^{1/2}\bar{u}_i^a\,\Delta t \tag{43}$$

$$\frac{M_i^a - M_{i-1}^a}{r_i^3 - r_{i-1}^3} = \frac{4\pi}{3}\rho_{i-1/2}^a \tag{44}$$

$$\frac{\bar{u}_i^a-(\bar{u}_i^a)^n}{\Delta t}+\bar{u}_i^a\frac{\bar{u}_{i+1}^a-\bar{u}_i^a}{r_{i+1}-r_i}\left[\frac{\bar{u}_i^a-\bar{u}_{i-1}^a}{r_i-r_{i-1}}\right]+\left(\frac{\alpha_{i+1/2}^a+\alpha_{i-1/2}^a}{2}\right)\times\frac{\ln(\rho^a\alpha^a)_{i+1/2}-\ln(\rho^a\alpha^a)_{i-1/2}}{r_{i+1/2}-r_{i-1/2}}+\frac{(\alpha^a-\beta^a)_{i-1/2}+(\alpha^a-\beta^a)_{i+1/2}}{r_i}+\frac{G}{r_i^2}\sum_{b=1}^{N}M_i^b=\left|\frac{d\bar{u}_i^a}{dt}\right|_{\text{coll}}\tag{45}$$

$$\frac{\alpha_{i-1/2}^a-(\alpha_{i-1/2}^a)^n}{\Delta t}+\bar{u}_i^a\frac{\alpha_{i+1/2}^a-\alpha_{i-1/2}^a}{r_{i+1/2}-r_{i-1/2}}\times\left[\frac{\alpha_{i-1/2}^a-\alpha_{i-3/2}^a}{r_{i-1/2}-r_{i-3/2}}\right]+2\alpha_{i-1/2}^a\frac{\bar{u}_i^a-\bar{u}_{i-1}^a}{r_i-r_{i-1}}+\frac{1}{\rho_{i-1/2}^a}\times\frac{\begin{pmatrix}(\rho_{i-1/2}^a\rho_{i+1/2}^a)^{1/2}\varepsilon_i^a\\-(\rho_{i-3/2}^a\rho_{i-1/2}^a)^{1/2}\varepsilon_{i-1}^a\end{pmatrix}}{r_i-r_{i-1}}+2\frac{\varepsilon_{i-1}^a+\varepsilon_i^a}{r_{i-1}+r_i}\left(1-\frac{2\beta_{i-1/2}^a}{3\alpha_{i-1/2}^a}\right)=\left|\frac{d\alpha_{i-1/2}^a}{dt}\right|_{\text{coll}}\tag{46}$$

$$\frac{\beta_{i-1/2}^a-(\beta_{i-1/2}^a)^n}{\Delta t}+\bar{u}_i^a\frac{\beta_{i+1/2}^a-\beta_{i-1/2}^a}{r_{i+1/2}-r_{i-1/2}}\times\left[\frac{\beta_{i-1/2}^a-\beta_{i-3/2}^a}{r_{i-1/2}-r_{i-3/2}}\right]+2\beta_{i-1/2}^a\frac{\bar{u}_i^a+\bar{u}_{i-1}^a}{r_i+r_{i-1}}+\frac{1}{3\rho_{i-1/2}^a}\frac{\begin{pmatrix}\{(\beta^a\rho^a/\alpha^a)_{i-1/2}(\beta^a\rho^a/\alpha^a)_{i+1/2}\}^{1/2}\varepsilon_i^a\\-\{(\beta^a\rho^a/\alpha^a)_{i-3/2}(\beta^a\rho^a/\alpha^a)_{i-1/2}\}^{1/2}\varepsilon_i^a\end{pmatrix}}{r_i-r_{i-1}}+\frac{4\beta_{i-1/2}^a}{3\alpha_{i-1/2}^a}\frac{\varepsilon_{i-1}^a+\varepsilon_i^a}{r_{i-1}+r_i}=\left|\frac{d\beta_{i-1/2}^a}{dt}\right|_{\text{coll}}\tag{47}$$

$$\frac{\varepsilon_i^a-(\varepsilon_i^a)^n}{\Delta t}+\bar{u}_i^a\frac{\varepsilon_{i+1}^a-\varepsilon_i^a}{r_{i+1}-r_i}\left[\frac{\varepsilon_i^a-\varepsilon_{i-1}^a}{r_i-r_{i-1}}\right]+3\varepsilon_i^a\frac{\bar{u}_{i+1}^a-\bar{u}_i^a}{r_{i+1}-r_i}+\frac{3}{2}\frac{(\alpha_{i+1/2}^a)^2-(\alpha_{i-1/2}^a)^2}{r_{i+1/2}-r_{i-1/2}}+\frac{2}{\rho_{i+1/2}^a+\rho_{i-1/2}^a}\times\frac{\rho_{i+1/2}^a\xi_{i+1/2}^a-\rho_{i-1/2}^a\xi_{i-1/2}^a}{r_{i+1/2}-r_{i-1/2}}+\frac{\xi_{i-1/2}^a+\xi_{i+1/2}^a}{r_i}\times\left(1-\frac{\beta_{i-1/2}^a+\beta_{i+1/2}^a}{\alpha_{i-1/2}^a+\alpha_{i+1/2}^a}\right)=\left|\frac{d\varepsilon_i^a}{dt}\right|_{\text{coll}}\tag{48}$$

$$\frac{\xi_{i-1/2}^a-(\xi_{i-1/2}^a)^n}{\Delta t}+\bar{u}_i^a\frac{\xi_{i+1/2}^a-\xi_{i-1/2}^a}{r_{i+1/2}-r_{i-1/2}}\left[\frac{\xi_{i-1/2}^a-\xi_{i-3/2}^a}{r_{i-1/2}-r_{i-3/2}}\right]+4\xi_{i-1/2}^a\frac{\bar{u}_i^a-\bar{u}_{i-1}^a}{r_i-r_{i-1}}+3(\varepsilon_i^a+\varepsilon_{i-1}^a)\times\frac{(\alpha_{i-1/2}^a\alpha_{i+1/2}^a)^{1/2}-(\alpha_{i-3/2}^a\alpha_{i-1/2}^a)^{1/2}}{r_i-r_{i-1}}+4\alpha_{i-1/2}^a\frac{\varepsilon_i^a-\varepsilon_{i-1}^a}{r_i-r_{i-1}}=\left|\frac{d\xi_{i-1/2}^a}{dt}\right|_{\text{coll}}.\tag{49}$$

In these equations a $n$ superscript stands for the value of the functions at time $t_n$, while the other functions are taken at time $t_{n+1}=t_n+\Delta t$. The subscripts indicate the grid points $r_i$ (or the intermediate points between two adjacent grid points, $r_{i-1/2}$), where the moments are evaluated. In order to evaluate the even moments $\rho_a$, $\alpha_a$, and $\beta_a$ at the grid points $r_i$ in the expressions for the collision terms of the odd moments (Eqs. (35), (38)), geometrical interpolation ($a_i=(a_{i-1/2}a_{i+1/2})^{1/2}$) has been used.

The expressions inside square brackets in Eqs. (44)–(49) mean that the difference expression for terms like $\bar{u}_a\partial/\partial r$ must be written in a different form, depending on the flux sign, $\bar{u}_a$, in order to avoid numerical instabilities [30]. When the mass flux is inwards ($\bar{u}_a<0$), the gradient must be written according to the expression without square brackets, while for those points where $\bar{u}_a>0$, the expression inside square brackets must be used. Thus, it is necessary to know the $\bar{u}_a$ sign in each grid point in order to properly choose the expression for the gradients. However, if this is done during the process of numerically solving the set of difference equations for one time step, the $\bar{u}_i^a$ functions could change their sign from one iteration to another, giving rise to problems of convergence. These problems can be avoided by choosing the gradient structure according to the $(\bar{u}_i^a)^n$ sign, obtained in the previous time step, instead of the $\bar{u}_i^a$, sign.

The difference equations (44)–(49) are used for $i=2, 3, \ldots, N_r-1$, where $N_r$ is the number of $r$ grid points. Equation (43) gives us the $M_a(r)$ functions at each time step.

In order to close the system of difference equations, boundary conditions at the end points of the $r$ interval must be given. Two different situations can be envisaged at $r=R_{\max}\equiv r_{N_r}$:

(a) *Reflecting wall condition.* This boundary condition implies that the self-gravitating system is isolated and that no exchange of matter or energy occurs across the wall. In consequence, the total mass and energy of the system are exactly conserved along the evolution. Mathematically, the reflecting wall condition demands that the odd moments be zero at $R_{\max}(\bar{u}^a_{N_r}=\varepsilon^a_{N_r}=0)$. This condition is somewhat artificial, but it allows us to test the accuracy of the numerical calculation (see below).

(b) *Absorbing wall condition.* In a self-gravitating system, energetic enough particles which reach the outermost region of the cluster can escape the gravitational force. This vaporization process is equivalent to placing a wall at $r=R_{\max}$ which absorbs any particle reaching this position. Mathematically this is done by truncating the radial velocity distribution function, at the boundary, for negative velocities. A particular choice of this distribution results in a particular relationship between the odd and even moments at this point, which closes the system of difference equations. In the absence of any information about this distribution, we have opted for the simplest choice: a truncated normal distribution

$$f^a(u)\propto\begin{cases}\exp[-u^2/2\alpha_a], & \text{if } u\geqslant 0\\ 0, & \text{if } u<0.\end{cases} \tag{50}$$

The first- and third-order moments of these distributions are

$$\bar{u}^a_{N_r}=\left(\frac{2}{\pi-2}\right)^{1/2}(\alpha^a_{N_r})^{1/2} \tag{51}$$

$$\varepsilon^a_{N_r}=\frac{2-\pi/2}{(\pi/2-1)^{3/2}}(\alpha^a_{N_r})^{3/2}. \tag{52}$$

If we had considered a different distribution function, we would have obtained different numerical factors, but still we would have $\bar{u}^a_{N_r}\propto(\alpha^a_{N_r})^{1/2}$ and $\varepsilon^a_{N_r}\propto(\alpha^a_{N_r})^{3/2}$. Fortunately, the value of these numerical factors does not significantly affect the subsequent evolution of the self-gravitating system.

Concerning the center of the configuration ($r_0\equiv r=0$), the reflecting wall condition has to be used because there are not sources or sinks of matter, so the particles can cross the center.

The difference equations (44)–(49) plus the boundary conditions at $r=0$ and $r=R_{\max}$ form a set of $N_E=6\times N\times N_r$ nonlinear algebraic equations with the same number of unknown functions, which has to be solved at each time step.

The accuracy of the calculations increases with $N_r$, but the computing time required to solve a time step grows as $N_r$, so that it is necessary to attain a compromise between accuracy and rapidity of the calculations. In the model of galaxy clusters we have computed, we have taken $N_r=70-90$, $N=4-10$, giving $1680\leqslant N_E\leqslant 5400$.

The standard Newton–Raphson technique has been used to solve the set of algebraic equations. The Jacobian matrix is of order $N_E$ with many of its elements equal to zero, and some others varying several orders of magnitude from the central regions to the outermost regions of the system. To calculate its inverse matrix we have used the Henyey [31] elimination procedure, largely used in the numerical solution of the equations of stellar evolution [32]. With this technique, instead of evaluating and storing all the elements of the matrix at the same time, they are handled blockwise so that, on one hand only the terms corresponding to the functions evaluated at $i-1$, $i$, and $i+1$ grid points are calculated and used simultaneously, and on the other hand, we deal with numbers of the same order of magnitude avoiding accuracy problems.

A particularity of our computational scheme is that the elements of the Jacobian matrix have been numerically evaluated at each time step. This has the advantage that it gives an enormous flexibility to the code under possible changes of the difference equations or boundary conditions. This also allows us to introduce new physical phenomena with very few changes of the code. By contrast, the computing time for each iteration grows. No relevant numerical instabilities have been found due to this numerical computation of the Jacobian matrix.

The trial solution for the Newton–Raphson method at each time step has been obtained by extrapolating the solution found for the two previous time steps. Linear and linear-logarithmic extrapolations have been used for the odd and even moments, respectively.

We consider that the solution to the nonlinear algebraic difference equations is achieved when the relative corrections to the even moments $\delta\rho^a_i/\rho^a_i$, $\delta\alpha^a_i/\alpha^a_i$, and $\delta\beta^a_i/\beta^a_i$, at every grid point, are less than $10^{-8}$. No more than seven iterations are necessary, in the worse cases, to achieve this accuracy. Actually, only three to five iterations are needed to get an accuracy better than $10^{-6}$ in most of the grid points.

The time step $\Delta t$ between two consecutive models has been taken to be variable. Its choice depends on how fast the convergence of the previous model is attained. This rapidity has been measured by the number of iterations needed and the maximum corrections to the trial solutions at the final iteration.

The computing code makes it possible to consider an arbitrary number of different mass subsystems, limited only by the storage capacity of the computer where it runs. The storage requirements grow like $N^2$. For a model with $N=4$ and $N_r=100$, this requirement is approximately 150K words in double precision.

The CPU time per iteration depends on the architecture

**TABLE I**

CPU Time for a Newton–Raphson Iteration, Using the Henyey Technique for the Inversion of the Jacobian Matrix, in Two Different Computers as a Function of the Number of Mass Subsystems

| $N$ | IBM-4381 (scalar) double precision | CRAY-XMP/14se (vectorial) single precision |
|---|---|---|
| 2 | 3.4s | 0.4s |
| 4 | 20.0s | 1.2s |
| 8 | 130s | 4.6s |
| 10 | 241s | 7.6s |

of the computer one uses. In computers with scalar processing, it grows as $N^3$, while in vectorial computers, it grows as $N^2$ when the code is fully vectorized. We have run the code in two different machines, one scalar (IBM-4381), with 0.98 Mflops double precision linpack, and the other with vectorial facilities (CRAY-XMP/14se) with 53 Mflops linpack, with a CFT77 fortran compiler. The times per iteration for a model with different mass subsystems and $N_r = 50$ in both computers are given in Table I. The computing time per iteration grows linearly as $N_r$ in scalar as well as in vectorial computers.

The accuracy of the code has been tested in two different ways: (a) First, its ability to maintain unchanged along the evolution those physical magnitudes which are invariants with a perfect reflecting wall boundary condition (such as the total mass of the system and the total energy). Our code fulfills these requirements, with a difference in the total mass satisfying the inequality $|\Delta M_T/M_T| < 10^{-16}$. The conservation of the total energy, $E_T$, is less accurate. For the most part of the time evolution, $|\Delta E_T/E_T| \lesssim 10^{-4}$. (b) We have also compared the results produced by our code with those produced with other codes found in literature, in the case of no mass spectrum [14, 15] and with a mass spectrum [33]. In both cases, using the same moment equations and the same initial model, the results agree quite well.

## 4. A PRACTICAL APPLICATION: RICH GALAXY CLUSTERS EVOLUTION

The system of differential equations in partial derivatives (44)–(49), with collision terms given by (35)–(39) can be used to study the dynamical evolution of any self-gravitating system with spherical symmetry in the two-body relaxation phase, once the initial conditions and the mass-spectrum are given. In order to show the physical relevance of the hypothesis of our model (namely, the existence of a mass spectrum, with a population a very light particles, and the anisotropy of the distribution function in the momentum space), here we briefly present some results of the computation of rich galaxy clusters evolution using this numerical method. For a more detailed analysis the reader should consult Refs. [20, 21].

As the initial configuration of our system we have taken the output of the violent relaxation phase [34]: the distribution function is nearly Maxwellian, so that no anisotropy will be initially present and the odd moments will be zero. Moreover, during the violent relaxation stage, the cluster can be considered as collisionless, so that no mass segregation will exist in the initial model. Among all the possible configurations fulfilling these requirements, King models have been chosen [35] because they properly fit the present density profiles of rich clusters of galaxies and we know that dynamical evolution implies a contraction of the core radius, $R_c$, but not a change in the slope of the density profiles, except for the more massive galaxies [21]. The core radius $R_c$ is defined by the equation $\sigma(R_c) = \sigma(0)/2$, where $\sigma(s)$ is the projected galaxy number density. The initial King models are characterized by three parameters: (i) the initial core radius $R_c$, (ii) the dimensionless gravitational potential at the cluster center $W_o$, and (iii) the total cluster mass $M_T$.

The mass spectrum of galaxy clusters is not observationally known. However, their observed differential luminosity functions is well fitted by the Schechter [36] function:

$$N(L)\,dL \propto \left(\frac{L}{L^*}\right)^{-\gamma} \exp\left(-\frac{L}{L^*}\right) d\left(\frac{L}{L^*}\right), \qquad (53)$$

where $\gamma \simeq 5/4$ and $L^* = 4.7 \times 10^{10} L$.

Assuming that the mass-luminosity ratio, $M/L$, is the same for all galaxies and that, moreover, it remains unchanged along the cluster evolution, we obtain the Schechter mass-spectrum

$$N(m)\,dm \propto \left(\frac{m}{m^*}\right)^{-\gamma} \exp\left(-\frac{m}{m^*}\right) d\left(\frac{m}{m^*}\right), \qquad (54)$$

where $m^*$ is the mass of galaxies with luminosity $L^*$ and is fixed by the $M/L$ value, which is another free parameter of the model. The fifth free parameter is the fraction of the cluster total mass which is in the form of very light particles:

$$\eta \equiv \frac{M_{\text{light}}}{M_T}. \qquad (55)$$

The galaxy mass range in our models has been taken to be

$$0.025 \leqslant m/m^* \leqslant 21. \qquad (56)$$

This mass interval has been divided into $N = 3$ subintervals of the same length in a logarithmic scale. All the particles in

each subinterval have been assumed to have the same mass, equal to the average mass value in the corresponding subinterval. These mass groups have been termed $a = 1$, 2, and 3 in order of decreasing average mass, and $a = 4$ stands for the very light particles subsystem.

The moment equations can be made dimensionless by taking as variables $X = r/R_c$ and $\tau = t/T_{r_0}$, where $T_{r_0}$ is defined as

$$T_{r_0} = \frac{\pi}{6} \frac{(M_T/\mu_{\max})^{1/2} R_c^{3/2}}{G^{1/2} m^* \ln [(2\pi/3)(X_{\max} M_T/\mu_{\max} m^*)]}. \quad (57)$$

and measures the relaxation time at the cluster center in the King model [25, 35]. In the above definition $X_{\max} = R_{\max}/R_c$ and $\mu(X) = 4\pi/9\ X^2\ dW/dX$ ($\mu_{\max} = \mu(X_{\max})$).

Dimensionless initial models are then characterized by the mass spectrum, the $W_o$ parameter and the effective number of galaxies: $N_{\text{eff}} = (1-\eta)\, M_T/m^*$. Their interest rests on the fact that they are defined by a set of three parameters instead of five and that the general features of the evolution are best described in a dimensionless language.

The most fundamental of these features is that the final stage of the dynamical evolution is always a situation of gravothermal catastrophe, characterized by an increase of the central density which becomes higher and higher in shorter and shorter time intervals. In multimass systems, the lack of energy equipartition among massive and light particles results in an acceleration of the process of gravothermal catastrophe relative to the monomass case. The most massive galaxies decouple from the lighter ones and they evolve independently as a monomass system to their collapse, which, in turn, induces the collapse of lighter galaxies.

The effects of the presence of a population of very light particles in the cluster dynamics, are well expressed by the $\alpha_a(X, \tau)$ profiles. In Fig. 1 we show the profile corresponding to the most massive group of particles, $\alpha_1$, for $\eta = 0$ (no light particles) and for $\eta = 0.9$. Values for the parameters $W_o = 9$ and $N_{\text{eff}} = 625$ have been chosen to draw these figures. The time variable $\tau$ has been normalized to the *collapse time*, $\tau_{cc}$, that is defined as the time needed for the density to become infinity at the center of the cluster. Our code is able to follow the evolution up to $\tau/\tau_{cc} \gtrsim 10^{-3}$, which is equivalent to an increase in the central density for the most massive particles, relative to its initial value, greater than $10^6$. At this time, the dimensionless functions $c_n^a \simeq 1$ (Eqs. (19)–(21)) and, as we mentioned in Section 2, the approximation made to close the system of moment equations no longer holds.

It is clear from these figures that the central cluster regions travel along their evolution by three different phases: first, a quick $\alpha_1$ decrease, more pronounced for high $\eta$ values; then, an interval where $\alpha_1$ is roughly constant, and, finally, a very fast increase of $\alpha_1$. A central decrease of the $\alpha_1$ profile when $\eta = 0.9$ is apparent from Fig. 1b. Also $\alpha_2$

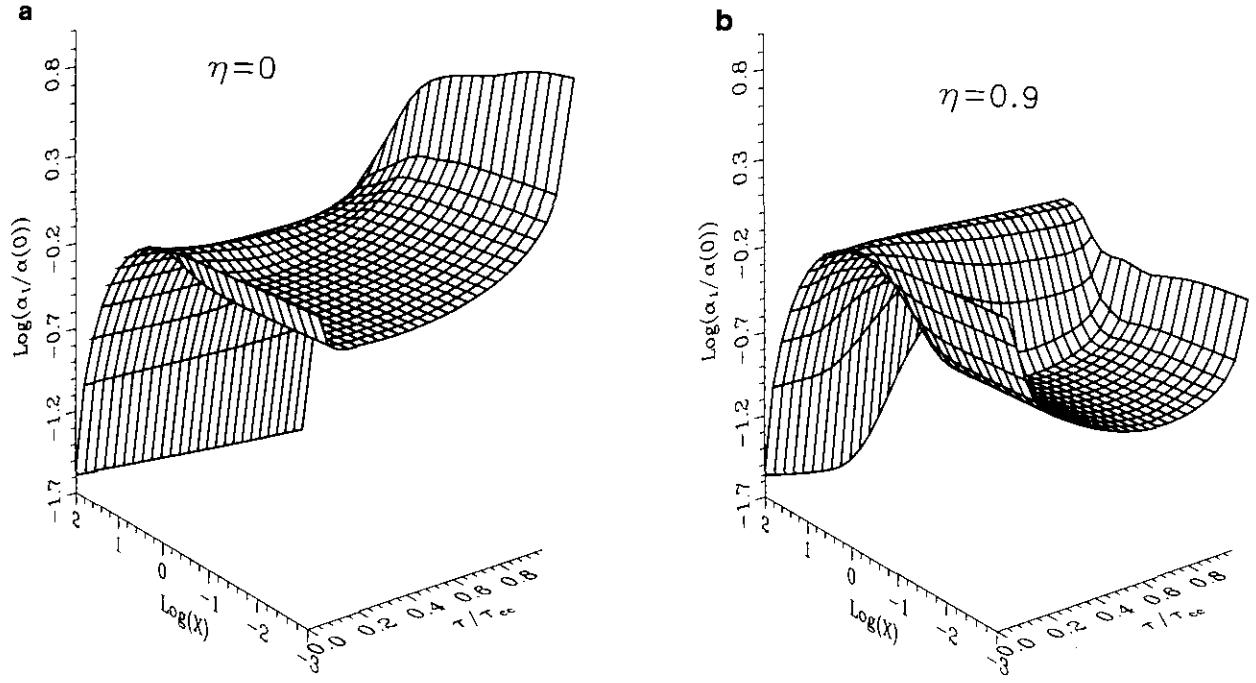


**FIG. 1.** Radial velocity dispersion profile for the most massive group of particles as a function of the dimensionless variables $X = r/R_c$ and $\tau = t/T_{r_0}$, in units of the initial central value $\alpha(0)$. The initial model is a King model with $W_0 = 9$ and $N_{\text{eff}} = 625$: (a) Model with no background of light particles ($\eta = 0$); (b) Model with $\eta = 0.9$.

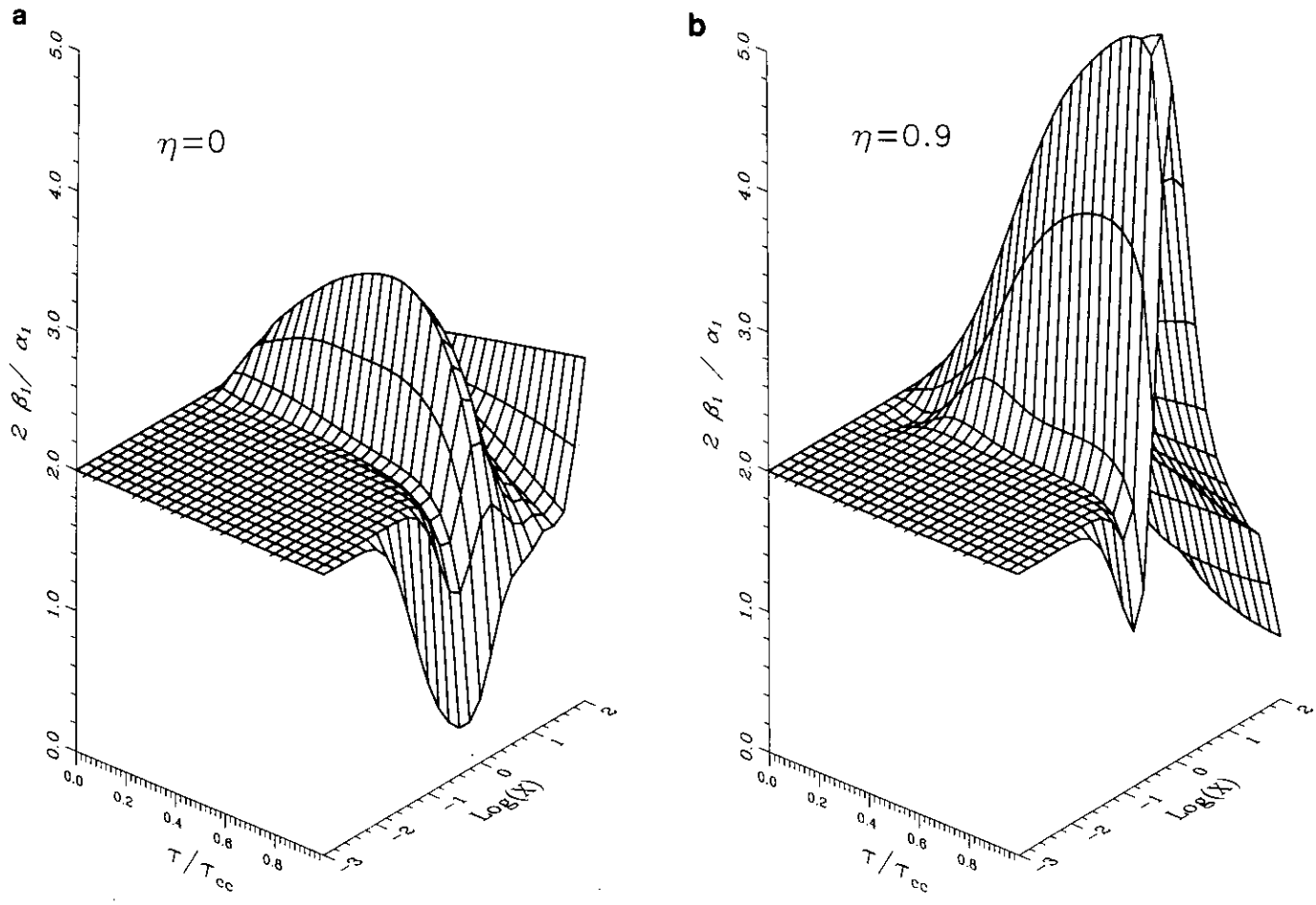


**FIG. 2.** Anisotropy factor $(2\beta_1/\alpha_1)$ for the most massive group of particles as a function of the dimensionless variables $X$ and $\tau$ for the same models as in Fig. 1: (a) Model with $\eta=0$; (b) Model with $\eta=0.9$. The initial model in both cases is isotropic.

decreases slightly, while $\alpha_3$ and $\alpha_4$ remain approximately constant along the evolution. This is a feature which is found in the observed projected velocity dispersion profiles of some galaxy clusters [21]. This central decrease of the $\alpha_1$ profile does not occur when light particles are not present (Fig. 1a). This is an important difference between the $\eta=0$ and $\eta=0.9$ case. Physically, the evolution of the $\alpha_a$ (and $\beta_a$) moments are caused by the competition among four processes: energy equipartition, convective and conductive heat transport, and the contractions and expansions of the configuration. The kinetic energy loss of the more massive galaxies which characterizes the first phase of the evolution is caused by the tendency to energy equipartition. As a consequence, massive galaxies concentrate toward the center, gaining kinetic energy, which is again transferred to the light galaxies and particles. This is the second phase. When collisions become ineffective to transfer this kinetic energy, the tendency to energy equipartition is broken and the gravothermal catastrophe begins.

In self-gravitating systems, an anisotropy develops as a consequence of the evolution in the two-body relaxation phase. In Fig. 2 the evolution of the anisotropy factor, $2\beta_1/\alpha_1$ of the most massive group, for $\eta=0$ and $\eta=0.9$, has been depicted. The central zones $(X\lesssim 0.1)$ remain always isotropic, but an anisotropy appears in the outer regions. Massive galaxies preferentially move in the transverse direction in the interval $0.2\lesssim X\lesssim 5$. Lighter galaxies in this region present no changes for $\eta=0.9$ nor a depletion of the anisotropy factor when $\eta=0$.

## 5. CONCLUSIONS

In this paper we have presented a description of the stochastic model we have developed in order to study the dynamical evolution of self-gravitating astronomical objects. The model is a self-consistent generalization to the multimass and anisotropic case of the Fokker–Planck equation moment method [14].

We have also made a detailed description of the computing code built for numerically solving the equations of the model. More realistic situations, with the inclusion of other

physical processes rather than those that are purely gravitational, can also be treated within the framework of this code.

In order to show the physical importance of the assumptions in which the model is based (mass spectrum and anisotropy in the velocity distribution) we have presented a practical application of the code to the solution of various models, describing the dynamical evolution of a galaxy cluster with, and without, a continuous background of light particles. The numerical results show that the mass spectrum and the anisotropy in the velocity distributions have a remarkable effect on the dynamical evolution of these kinds of physical systems so that their inclusion is necessary if one wants to obtain a realistic model.

## ACKNOWLEDGMENTS

We acknowledge Dr. H. Loose who kindly provided us with his version of the Henyey routine and Dr. F. Elorza for useful discussions. We also thank the CICyT (Spain) for kindly allowing us access to the CRAY-XMP supercomputer of CASA, where part of the calculations were performed. This work has been partially supported by the Dirección General de Investigación Cientifica y Técnica (project number PB86-0292-C04-03).

## REFERENCES

1. S. D. M. White, *Mon. Not. R. Astronom. Soc.* **177**, 717 (1976).
2. S. Aarseth, in *Multiple Time Scales*, edited by, J. U. Brackbill and B. I. Cohen (Academic Press, New York, 1985), p. 377.
3. M. J. West and D. O. Richstone, *Astrophys. J.* **335**, 532 (1988).
4. L. Spitzer, Jr. and M. Hart, *Astrophys. J.* **166**, 511 (1971).
5. M. Hénon, *Astrophys. Space Sci.* **14**, 151 (1971).
6. L. Spitzer, Jr. and J. M. Shull, *Astrophys. J.* **201**, 773 (1975).
7. S. L. Shapiro, in *IAU Symposium 113, Dynamics of Star Clusters*, edited by J. Goodman and P. Hut (Reidel, Dordrecht, 1985), p. 373.
8. H. Cohn, *Astrophys. J.* **234**, 1036 (1979).
9. H. Cohn, *Astrophys. J.* **242**, 765 (1980).
10. D. Merritt, *Astrophys. J.* **262**, 24 (1983).
11. D. Merritt, *Astrophys. J.* **276**, 26 (1984).
12. H. Cohn, in *IAU Symposium 113, Dynamics of Star Clusters*, edited by J. Goodman and P. Hut (Reidel, Dordrecht, 1985), p. 161.
13. S. Inagaki and W. C. Saslaw, *Astrophys. J.* **292**, 339 (1985).
14. R. Larson, *Mon. Not. R. Astronom. Soc.* **147**, 323 (1970).
15. R. Larson, *Mon. Not. R. Astronom. Soc.* **150**, 93 (1970).
16. L. Angeletti and P. Giannone, *Mem. Soc. Astronom. Italiana* **47**, 245 (1976).
17. M. Saito and M. Yoshizawa, *Astrophys. Space Sci.* **41**, 63 (1976).
18. E. Bettwieser, *Mon. Not. R. Astronom. Soc.* **203**, 811 (1983).
19. E. Bettwieser and S. Inagaki, *Mon. Not. R. Astronom. Soc.* **213**, 4 (1985).
20. G. Yepes, R. Domínguez-Tenreiro, and R. del-pozo-Sanz, *Astrophys. J.* **373**, 336 (1991).
21. G. Yepes and R. Domínguez-Tenreiro, *Astrophys. J.* **387**, 127 (1992).
22. J. Silk, in *Cosmology and Particle Physics*, edited by E. Alvarez, R. Domínguez-Tenreiro, J. M. Ibáñez, and M. Quirós (World Scientific, Singapore, 1987), p. 35.
23. K. A. Olive, D. N. Schramm, G. Steigman, and T. P. Walker, *Phys. Lett. B* **236**, 454 (1990).
24. D. Lynden-Bell and R. Wood, *Mon. Not. R. Astronom. Soc.* **138**, 495 (1968).
25. S. Chandrasekhar, *Rep. Modern Phys.* **45**, 1 (1943).
26. J. Binney and S. Tremaine, *Galactic Dynamics* (Princeton Univ. Press, Princeton, NJ, 1987).
27. M. N. Rosenbluth, W. H. MacDonald, and D. L. Judd, *Phys. Rev.* **107**, 1 (1957).
28. G. Yepes, Ph.D. thesis, Universidad Autónoma Madrid, 1989 (unpublished).
29. R. Courant, K. O. Friedrichs, and H. Lewy, *IBM J. Res. Develop.* **215** (1967).
30. R. D. Richtmyer and K. W. Morton, *Difference Methods for Initial Value Problems* (Wiley–Interscience, New York, 1967).
31. L. G. Henyey, J. E. Forbes, and N. L. Gould, *Astrophys. J.* **139**, 306 (1964).
32. R. Kippenhahn, A. Weigert, and E. Hofmeister, *Methods Comput. Phys.* **7**, 129 (1967).
33. L. Angeletti and P. Giannone, *Astrophys. Space Sci.* **50**, 311 (1977).
34. D. Lynden-Bell, *Mon. Not. R. Astronom. Soc.* **136**, 101 (1967).
35. I. R. King, *Astronom. J.* **71**, 64 (1966).
36. P. L. Schechter, *Astrophys. J.* **203**, 297 (1976).